Title

Disruption of transcription–translation coordination in Escherichia coli leads to premature transcriptional termination

Journal

Nature Microbiology, 4(12)

ISSN

2058-5276

Authors

Zhu, Manlu
Mori, Matteo
Hwa, Terence
et al.

Publication Date

2019-12-01

DOI

10.1038/s41564-019-0543-1

Peer reviewed

HHS Public Access

Author manuscript

Nat Microbiol. Author manuscript; available in PMC 2020 June 01.

Published in final edited form as:

Nat Microbiol. 2019 December ; 4(12): 2347–2356. doi:10.1038/s41564-019-0543-1.

Disruption of transcription-translation coordination in *Escherichia coli* leads to premature transcriptional termination

Manlu Zhu[1], **Matteo Mori**[2], **Terence Hwa**[2], **Xiongfeng Dai**[1]

[1]School of Life Sciences, Central China Normal University, Wuhan, China

[2]Department of Physics, University of California at San Diego, La Jolla, California, USA

Introductory paragraph

Tight coordination between transcription and translation is crucial to maintaining the integrity of gene expression in bacteria. How bacteria manage to coordinate these two processes remains unclear. Possible direct physical coupling between the RNA polymerase and ribosome has been intensely investigated in recent years. Here, we quantitatively characterize the transcriptional kinetics of *E. coli* in different growth conditions. Transcriptional and translational elongation remain coordinated under various nutrient conditions as previously reported. However, transcriptional elongation was not affected under antibiotics that slowed down translational elongation. The same was found by introducing non-sense mutation that completely dissociated transcription from translation. Our data thus provide direct evidences showing that translation is not required to maintain the speed of transcriptional elongation. In cases where transcription and translation are dissociated, our study provides quantitative characterization of the resulting process of premature transcriptional termination (PTT). PTT-mediated polarity caused by translation-targeting antibiotics substantially affected the coordinated expression of genes in several long operons studied, contributing to important physiological effects of these antibiotics. Our results also suggest a model in which the coordination between transcriptional and translational elongation under normal growth conditions is implemented by ppGpp.

INTRODUCTION

The transcription and translation processes are tightly coordinated in bacterial cells[1,2], as demonstrated by the same elongation speeds of RNA polymerase (RNAP) with ribosomes in different growth conditions[2–4]. The loss of coordination in cases such as nonsense mutation[5] or ribosome pause[6] can lead to premature transcriptional termination, affecting the expression of downstream genes as demonstrated in the “polarity” phenomenon[5,7,8]. Despite the importance of transcriptional-translational coordination, underlying mechanisms remains

Correspondence: hwa@ucsd.edu; daixiongfeng@mail.ccnu.edu.cn.

Author contribution

X.D and T. H designed the study. M.Z and X.D performed experiments. M.Z, M.M, T.H and X.D analyzed the data. X.D, T.H and M.Z wrote the paper.

Data availability: the key data that support the findings of this study are summarized in supplementary tables. Some other details are available from the corresponding author upon request.

Competing interests statement

The authors declare no conflicts of interests.

unclear. It is known that the elongating RNAP is closely followed by a trailing ribosome during gene expression[2,9,10]. Previous work suggested that the trailing ribosome could effectively push the elongating RNAP by inhibiting the spontaneous backtracking of the latter, thereby matching the speed of RNAP with ribosome in many growth conditions[4]. Structural and biochemical studies have provided evidences that ribosome can interact with RNAP, either directly[9,11,12] or indirectly by the bridging of NusG protein or its homolog, RfaH[13–15], providing a physical mechanism of the ribosome-RNAP coupling. The direct physical coupling picture is inconsistent with results on hammerhead-catalyzed cleavage of mRNA which did not affect protein synthesis in rich medium[16]. Thus, it remains unclear whether and under what conditions direct coupling may occur, and if not, how bacterial cells manage to coordinate transcriptional and translational elongation.

Here, we quantitatively investigate the transcription-translation coordination of *E. coli* under various growth conditions. We show that transcriptional elongation speed is unaffected when translation is slowed down by antibiotics or completely abolished by nonsense mutation, demonstrating that translating ribosome (hence physical coupling) is not required at all for maintaining the speed of transcriptional elongation. Further investigations support a model in which the coordination of transcriptional and translational elongation under nutrient limitation is mediated by ppGpp. Importantly, our study quantitatively elucidates the effect of premature transcriptional termination (PTT) that results from the dissociation between transcription and translation upon treatment of translation-inhibiting antibiotics, which contributes to important physiological consequences of antibiotics.

RESULTS

Quantitative characterization of transcriptional kinetics

We first established a versatile ‘multi-probe’ approach for quantifying the mRNA transcriptional kinetics. We measured the induction kinetics of *lac*Z mRNA upon IPTG addition for exponentially growing *E. coli* K-12 NCM3722 cells by qRT-PCR. Seven pairs of primers were used to detect the synthesis of different *lacZ* mRNA sub-regions. For example, primer P297 detects near 5’-head region of the mRNA and the P3105 primer detects near 3’-tail region of the *lacZ* mRNA (Supplementary Figure 1). The *lacZ* mRNA abundances as detected by these seven primers all increased linearly with time after some delays (Figure 1A). The “waiting time” required for transcribing each mRNA sub-region j (e.g., j = 297 for primer P297), T_j, was directly deduced from the linear fit of each induction curves. Plotting each T_j against its position j along the *lacZ* mRNA, we obtained a linear relation (Figure 1B), the slope of which gives the transcriptional elongation speed, 15.9 ± 0.4 codons/s, being quantitatively consistent with previous estimates[3,17,18]. The X-intercept, 8 ± 1 s, denotes the time (T_{ini}) needed to initiate *lacZ* mRNA transcription after IPTG induction, including IPTG penetration, LacI depression and RNAP transcriptional initiation. These results are highly reproducible (Supplementary Figure 2).

Quantitative comparison of transcriptional and translational elongation speeds

We next characterized LacZ protein induction[19–21] and *lacZ* mRNA induction simultaneously to investigate transcriptional-translation coordination. As exemplified in

Figure 1C for cells grown in glucose medium, the waiting time for the synthesis of the complete LacZ protein was similar to that for the synthesis of the complete *lacZ* mRNA, suggesting similar speeds for transcriptional and translational elongation. The translational elongation speed can be quantitatively deduced using the Schleif plot (Supplementary Figure 3)[22]. The result, 16.0 ± 0.3 aa/s, matches well with the transcriptional elongation speed obtained by the multiple-probe approach above.

Recent work shows that the translational elongation speed of *E. coli* drops moderately under nutrient limitation[20]. Here, we found that the transcriptional elongation speed also steadily decreased under poor nutrient conditions (Figure 1D), exhibiting the same dependence on growth rate as the translational elongation speed (Figure 1E; see also the comparison between transcriptional and translational kinetics in typical growth medium (Supplementary Figure 4). In particular, in the extreme poor condition (glycerol threonine medium, with doubling time ~20 hours), transcriptional elongation speed (8.6 ± 0.3 codons/s) and translational elongation speed (9.1 ± 0.2 aa/s) are both approximately half of the maximum elongation speeds obtained for rapidly growing cells (Figure 1E and 1F). In summary, the above results recapitulate earlier finding by Vogel and Jensen[3], that *E. coli* maintains a tight coordination between transcriptional and translational elongation under nutrient limitation, but determined at a broader range of growth rates.

Maintenance of transcriptional elongation speeds under chloramphenicol inhibition

Translation-inhibiting antibiotic is potentially an effective way to perturb the effect of translation on transcriptional elongation. Proshkin *et al*[4] reported that a low dose of chloramphenicol (Cm, 1 μg/mL or 3 μM) slowed down translational elongation by ~35% with similar drop in the transcriptional elongation speed for *E. coli* MG1655 cells growing in LB medium, supporting their model of transcription-translation coupling via ribosome pushing RNAP. However, the reported slowdown of translation elongation by Cm is inconsistent with the result of Refs.[19,20], which found the translational elongation speed to be maintained under Cm treatment in various conditions (Supplementary Figure 5).

As the outcome of the Cm study is key to this leading model of transcription-translation coupling, we repeated this investigation for *E. coli* NCM3722 cells growing in glucose medium with 8 μM Cm (Supplementary Table 1). Although the overall synthesis rate of LacZ protein was significantly reduced by Cm (Figure 1G), the waiting time for the appearance of first protein was hardly changed from that of no-drug condition (inset of Figure 1G), indicating the maintenance of translational elongation speed under Cm treatment. Similarly, the overall synthesis rate of *lacZ* mRNA was reduced by Cm (filled purple circles in Figure 1H). However, the waiting time for the appearance of the first full-length *lacZ* mRNA was also not affected by Cm, indicating that the transcriptional elongation speed was also not reduced (Figure 1H), as quantitatively demonstrated by the multi-probe assay (Figure 1I). Therefore, Cm does not affect either the transcriptional or translational elongation speeds. We further repeated the experiment for MG1655 cells growing in LB medium with/without 3 μM Cm as done in Ref. 4. Again we found transcriptional and translational elongation speeds to be maintained under Cm treatment (Supplementary Figure 6). The difference in the conclusion between our measurements and

those of Ref. 4 may be attributed to the larger uncertainty of their dot-blotting data and the longer time interval (20 s) used in their sample collection.

In addition to Cm, recent work has also shown that sublethal doses of erythromycin (Ery) do not reduce the translational elongation speed of *E. coli* cells[20] (Supplementary Figure 7A). Here we found that transcriptional elongation speed was also not affected (Supplementary Figure 7B). In summary, the transcriptional and translational elongation speeds match well with each other in both normal conditions and including treatment of Cm and Ery.

Dissociation between transcription and translation under fusidic acid inhibition

Our results on Cm inhibition, while not supporting the ribosome-pushing RNAP model of Ref.[4], are not inconsistent with the model. To test the possibility of physical coupling, we turned to another antibiotic, fusidic acid (FA), which targets the ribosome translocation by inhibiting the recycling of EF-G[23,24]. FA causes the gradual slowdown of translational elongation at sublethal doses[20,21]. Unfortunately, both NCM3722 and MG1655 are insensitive to FA, so we turned to a fusidic acid permeable *E. coli* B/r strain AS19[23]. This strain has similar growth rate and ribosome content as NCM3722 in different medium (Supplementary Figure 8). As expected, translational elongation speed of AS19 cells dropped by 50% (~8 ± 0.2 aa/s) under sublethal FA treatment (1.2 mg/ml) in glucose medium (Figure 2A, Supplementary table 1). Strikingly, the waiting time for the appearance of the full-length *lacZ* mRNA was almost not affected by FA (Figure 2B), suggesting that transcriptional elongation was unaffected, as quantitatively demonstrated by the multi-probe assay (Figure 2C). Plotting *lacZ* mRNA induction with the Schleif plot directly demonstrates the shorter waiting time for generating the first intact *lacZ* mRNA compared to the first LacZ protein (Supplementary Figure 9A). A similar result was obtained for cells growing in glycerol medium (Figure 2D and supplementary Figure 9B). The transcription-translation dissociation was also observed at a lower dose of FA (0.3 μg/mL) where translational elongation speed was reduced (~12 aa/s) but transcriptional elongation speed was maintained (Figure 2D and supplementary Figure 9C). In summary, transcriptional elongation speed is maintained when translational elongation is slowed down by FA, indicating that ribosome-pushing is not required to maintain the transcriptional elongation speed, opposite to the expectation of the model of Ref. 4.

Effect of nonsense mutation on transcriptional elongation

To complement the study on FA where severe growth inhibitions occurred, we also characterized transcriptional elongation speed under nonsense mutation in which the trailing ribosomes are eliminated without causing any physiological perturbations. We introduced a stop codon at the 500th nucleotide after transcription start of *lacZ* to terminate translation. Multi-probe assay shows that the elongation speed is still indistinguishable from that of WT *lacZ* in glucose medium and aspartate ammonium medium (Figure 3A, 3B). These findings thus strongly reinforce the conclusion that ribosome is not required to maintain the elongation speed of RNAP.

The ability to measure transcriptional elongation speed of nonsense mutated-*lacZ* may be surprising given past work on the ‘polarity effect’[5,7], that the expression level of the

downstream gene was reduced substantially. However, inspection of our induction curves (Figure 3C) shows a substantial but graded reduction in the rate of local mRNA accumulation (black diamond in Figure 3D), allowing us to determine the transcriptional elongation speed accurately in the absence of translation with the first six primers. The position-dependent decline in local mRNA synthesis seen in Figure 3D is naturally attributed to the premature transcriptional termination (PTT) effect mediated by Rho[5,7], as supported by the fact that PTT was largely prevented by a specific Rho inhibitor, bicyclomycin (Bcm) (Figure 3E). The accuracy of the multi-probe assay allows us to quantify the spatial dependence of this Rho-dependent PTT effect for the first time: the mRNA synthesis rate of different sub-regions generally declined by ~50% over ~500 nt (black diamond in Figure 3D). An abrupt drop in transcriptional processivity can be obtained by inserting a transcriptional pause site[25,26] shortly downstream of the nonsense mutation, with ~80% drop in local mRNA accumulation rate immediately downstream of the pause site (Supplementary Figure 11, red triangles). This observation indicates that termination efficiency of Rho-mediated PTT is much lower than that of a designated Rho-dependent terminator.

PTT induced by translation inhibiting antibiotics

In contrast to the case of nonsense mutation, PTT is negligible under nutrient limitation where translation and transcription coordination is tightly maintained (red circle of Figure 3D, supplementary Figure 10). In the case of FA treatment where translation-transcription dissociation occurs, the synthesis rates of downstream *lacZ* mRNA sub-regions was reduced as well, displaying severe PTT (Figure 3F and Supplementary Figure 12A). For Cm and Ery treatment, although translational elongation speed still matches well with transcriptional elongation speed, severe PTT was still observed (Supplementary Figure 12B and 12C). We reasoned here that although transcription and translation are still coordinated for a fraction of normally elongating ribosomes, PTT would likely result from transcription-translation dissociation on mRNAs with stalled ribosomes (illustrated in supplementary Figure 12D). We developed a mathematical model of PTT in the presence of Cm-ribosome binding and found that a quantitative agreement of these distinct dataset can be obtained if the timescale for *in vivo* Cm-ribosome unbinding is 1~2 min (see Supplementary Note).

In all cases of treatment with translation inhibiting drugs (colored symbols in Figure 3G), PTT is less severe than that in the case of nonsense mutation (black diamond in Figure 3G), reflecting presumably partial coordination between transcription with the remnant translation activities of the ribosomes under drug treatment. *In vitro* studies have shown that there are five intrinsic *rut* sites (Rho-binding site) in the near 5' region of *lacZ* gene, locating at ~180, 220, 379, 421 and 463 base pairs downstream from the transcriptional start point[27]. In the case of nonsense mutation, those *rut* sites do not contribute to the PTT since the stop codon was introduced downstream of them. Moreover, all the data of Figure 3G shows a smooth attenuation of transcription compared to that induced by the pause site in supplementary Figure 11, indicating that those intrinsic *rut* sites do not contribute notably over the background PTT effect and should not be related to the PTT effect of antibiotic treatment.

We next extended the transcriptional kinetics study to downstream genes of the *lacZYA* operon with four additional primer pairs detecting the 5' and 3' region of the *lacY* and *lacA* mRNA (Supplementary Figure 1). In normal conditions where PTT within *lacZ* is negligible (Figure 1A), the synthesis rates in *lacYA* mRNA sub-regions were similar with that the 3'-tail of *lacZ* mRNA, indicating that transcriptional elongation was fully processive within the entire *lac* operon (Supplementary Figure 13A). In contrast, the synthesis rates of *lacYA* mRNA becomes progressively slower for culture under drug treatment, indicating that strong PTT occurred throughout the length of the *lac* operon (Figure 3H, Supplementary Figure 13BC), as quantitatively shown in Figure 3I. In summary, the transcription rate of a gene downstream is smaller than that of the upstream gene due to PTT under the treatment of translation inhibiting drugs. This is a quantitative generalization of the "polarity effect"[5,7] to the case of antibiotics.

Antibiotics induced polarity effect for ribosomal protein operons

We next tested the occurrence of similar antibiotic-induced "polarity effect" for the r-protein operons, whose synthesis significantly increased upon the treatment of translation-inhibiting antibiotics[20,23,28,29]. We focused on the expression of the two longest r-protein operons, S10 operon and Spc operon (Figure 4A and 4D) treated with sublethal doses of drugs. The mRNA abundance of r-protein indeed decreased along the length of the two operons (red symbols in Figure 4B, 4E), suggesting the occurrence of PTT effect. In contrast, no PTT was observed for cells grown in poor carbon sources (purple squares in Figure 4B, 4E) where transcription-translation coordination is maintained. For the protein abundances, although most r-proteins exhibit generally increasing trend with increasing Cm concentration[20,30], the abundance pattern of individual r-proteins is strongly dependent on their positions within the operon (Supplementary Figure 15). The abundances of individual r-proteins in S10 operon and Spc operon significantly dropped along the length of each operon (red circles in Figure 4C, 4F), displaying a similar trend as the transcription levels along the operon. In contrast, no PTT is detected for similar slow growth resulting from poor carbon or nitrogen sources (Figure S10), and the abundances of individual r-protein do not show appreciable positional dependences (purple squares and green triangles in Figure 4C and 4F). These results support the notion that antibiotics-induced PTT is responsible for disrupting the coordinated synthesis of individual ribosomal proteins along these operons.

Effect of ppGpp on transcriptional and translational elongation

Given that ribosome is not required to maintain the transcriptional elongation speed, we asked how transcriptional and translational elongation remained coordinated under nutrient limitation (Figure 1E). We focused on the role of the alarmone ppGpp[31], which was suggested to affect transcriptional elongation under starvation conditions[32–34] and was shown to inhibit transcriptional elongation *in vitro*[35,36]. We constructed a ppGpp up-regulation strain, FL56, allowing overexpression of a constitutively active RelA protein (called $RelA^+$, Figure 5A)[37]. $RelA^+$ overexpression resulted in elevated levels of ppGpp and inhibited cell growth[38,39] (Supplementary Figure 16A). Cell growth arrest occurred rapidly upon addition of 20 ng/mL cTc. At 20 min after the onset of growth arrest (Supplementary Figure 16B), we found both the transcriptional and translational elongation speeds decreased by ~50% (Supplementary Figure 16C–E). To remove possible interferences of translation on

transcription, we repeated the RelA$^+$ induction experiment for FL56 cells growing exponentially with FA, where transcription is dissociated from translation (Figure 2). Addition of 20 ng/mL cTc for ppGpp synthesis (black circles in Figure 5B) again reduces the transcriptional elongation speed by ~50% (circles in Figure 5C). For an intermediate level of induction (5 ng/mL cTc), transcriptional elongation speed exhibited an intermediate drop (triangles in Figure 5C). Thus, the transcriptional elongation speed can be gradually varied by titrating ppGpp synthesis. Given that the translational elongation speed was not affected by cTc addition (Figure 5D, blue bars in Figure 5E), these results establish that the transcriptional elongation speed is ppGpp-dose dependent independent of translation.

Co-variation of transcriptional elongation speed with RNA/protein ratio

Since ppGpp level is known to increase poor nutrient conditions[17,40,41], while increased ppGpp synthesis slows down transcriptional elongation (Figure 5E), the slowdown of transcriptional elongation under nutrient limiting conditions may simply be a result of increased ppGpp levels. In a simple model (Figure 6A), the coordination with translational elongation is explained by the fact that ppGpp also regulates the synthesis of the tRNA ternary complex[17,41,42], whose abundance dictates translational elongation speed under different nutrient conditions[20]. This model highlights the role of ppGpp as a coordinator by simultaneously modulating transcriptional and translational elongation under nutrient limitation.

We next seek to test this model quantitatively. The ppGpp is the primary factor that regulates ribosome synthesis in *E. coli*[17,20,23,41,43,44]. Under nutrient limited growth, the elevated ppGpp pool reduces the RNA/protein ratio, *R/P* (Supplementary Figure 17A and B)[17]. In contrast, ppGpp pool decreases under FA treatment[23], leading to the increase of *R/P*[23] (Figure 6B). Therefore, *R/P* can reasonably be used as an (inverse) indicator of the ppGpp pool. Under nutrient limitation alone, transcriptional and translational elongation speeds and *R/P* all decreased with decreasing growth rate (black circles in Figure 6B–D). Addition of sub-lethal doses of FA slowed down the translational elongation in various nutrient conditions (colored symbols of Figure 6C). In contrast, transcriptional elongation speed was maintained in glucose medium and even increased in poorer nutrient conditions (Figure 6D and Supplementary Figure 18). Strikingly, when we plotted the transcriptional elongation speed data against *R/P* data (the latter used here as the indicator of ppGpp), we found that the diverging data of transcriptional elongation speed versus *R/P* collapsed onto a single Michaelis-Menten curve (Figure 6E), being the same as previously found in the dependence of the translational elongation speed on *R/P* under nutrient limitation[20]. Transcriptional elongation speed follows the Michaelis-Menten dependence even when translational elongation speed deviates from it under FA treatment (Supplementary Figure S19). Thus, transcriptional elongation speed follows the *R/P* ratio, which reflects the ppGpp pool, regardless of the state of translational elongation.

DISCUSSION

In this study, we firmly establish that translation by a trailing ribosome is not required for maintaining the elongation speed of RNAP across growth conditions. Although ribosomes

can play the role of anti-backtracking[4], the data of fusidic acid and nonsense mutation indicate that such anti-backtracking is not required to maintain the transcriptional elongation speed *in vivo*. Our findings do not exclude the physical coupling between RNAP and the trailing ribosome. Given that the actual distance between RNAP and the first trailing ribosome may vary due to fluctuations in the two speeds, physical coupling could effectively limit the gap between RNAP and its trailing ribosome, thereby avoiding Rho-mediated PTT. However, the hypothetical bridges between RNAP and ribosome (observed in structure)[9] might not be strong enough to hold when translation slows down (e.g., under antibiotic treatment). Our results are also consistent with recent findings of the lack of difference between single- and multiple-rounds of translation[16], reflecting the lack of physical coupling. Thus, instead of physical coupling enabling the coordination of transcriptional and translational elongation, our results suggest that the coordination of the two elongation processes is necessary for the occurrence of physical coupling.

Our results support a global role of ppGpp in coordinating transcriptional and translational elongation speeds under nutrient limitation (Figure 6A). Under poor nutrient conditions, limitation in the charged tRNA levels due to elevated ppGpp level[45] reduces the translational elongation speed[17,20,41,42], resulting in the empirical Michaelis-Menten dependence of the translational elongation speed on *R/P*; see Supplementary Figure 17C and Ref.[20]. The relation between *R/P* and ppGpp pool implies a relation between the translation speed and the ppGpp pool (Supplementary Figure 17D). Since elevated ppGpp level directly inhibits the transcriptional elongation (Figure 5C)[35]. The degree of this inhibitory interaction can in principle be adjusted to match the relation between the ppGpp pool and the translational elongation speed. We analyzed the quantitative dependence of the transcriptional elongation speed on the ppGpp pool: Strikingly, the correlation between the ppGpp pool and transcription elongation speed obtained *in vivo* is quantitatively consistent with the inhibitory kinetics of ppGpp effect on the RNAP elongation *in vitro* (Supplementary Figure 17D, 17E)[35]. Thus, by adjusting the two parameters characterizing the interaction between ppGpp and RNAP elongation, the cell can readily match transcriptional and translational speeds without the need to finely adjust interaction for each nutrient condition.

Our work also brings to light the PTT-mediated polarity effect induced by antibiotics. According to previous model[4] where ribosome pushes RNAP to maintain the same elongation speeds, one would not expect to observe polarity in response to translation-inhibiting antibiotics. Instead, we find such antibiotics to dissociate translation from transcription, resulting in extensive polarity effect for long operons. PTT-mediated polarity resulted in ~50% attenuation of transcription of the r-protein operons (Figure 4), thereby significantly breaking the coordinated synthesis of individual r-proteins upon Cm treatment. The ~50% attenuation of a subset of r-proteins diminishes the number of functional ribosomes by 50%, since all r-proteins are required in equal amount in order to have a functional ribosome. It has been noted previously that non-coordinated synthesis of r-proteins inhibits ribosome assembly and generates inactive ribosome precursors[28,29,46]. Our results further show that a large fraction of r-proteins synthesized (from the upstream part of the long operons exhibiting polarity) are useless. It is known that up to 40% of cellular proteins are r-proteins under translation-inhibiting antibiotics[30]. If half of them are rendered useless due to dis-coordinated synthesis by the polarity effect, then as much as 20% of the

proteome is rendered useless, leading to a ~50% reduction in growth rate according to previous studies of proteome resource allocation[30,47]. Thus, PTT is an important consequence of these drugs, comparable to the direct effect they exert on inhibiting the translation process. By exposing these physiological problems arising from drug treatment, our results demonstrate the importance of coordination between transcriptional and translational elongation, which prevents PTT and hence prevents cells from the synthesis of useless proteins in normal growth conditions.

Finally, we caution that our results on polarity are derived from a limited study of a few long operons, specifically, the *lac* operon and the two ribosomal operons. Quantitative effects of polarity might also depend on the specific operons, on specific transcriptional pause sites (as seen in Supplementary Figure 11) and with contributions from factors such as Rho and global regulator, H-NS[48]. In addition, some operons (e.g. *hlyCABD*) contain certain DNA elements that could suppress transcription polarity within the operons[49]. In the future, systematic studies are necessary to fully elucidate the variation of polarity effects among different operons.

MATERIALS AND METHODS

Strains

The strains used in this study included wild type K-12 NCM3722 strain and B/r AS19 strain[23]. The AS19 strain is a membrane permeable strain that is sensitive to fusidic acid treatment, and was thus used for fusidic acid study.

To construct the *relA*$^{+}$ overexpression strain, FL56, the *relA*$^{+}$ coding sequence (coding the N-termini 455 amino acids of native *relA* gene) was PCR amplified, and inserted into the KpnI/XbaI sites of the pZE11-*lacZ* vector to replace the *lacZ* gene, generating the pZE11-*relA+* vector. The pZE11-*relA+*vector was co-transformed with the pZA31-TetR vector into the AS19 strain to obtain the ppGpp-up-regulating strain, FL56.

To construct a *lacZ* nonsense mutant strain, the native *lacZ* gene was PCR amplified and inserted into the KpnI/BamHI site of the pZA31-*luc* vector, obtaining pZA31-*lacZ* vector. A point mutation converting “G” (the 500th nucleotides from the transcription start site of *lacZ*) to “A” was introduced with PCR mutation to the *lacZ* gene in pZA31-lacZ vector, generating pZA31-*lacZ’* vector. pZA31-*lacZ’* was transformed into a NCM3722 *lacZ* deficient strain to obtain the lacZ nonsense mutant strain FL57.

Mediums

The growth media used in this study were MOPS-buffered medium containing 40 mM MOPS, 0.1 M NaCl, 4 mM Tricine (adjusted to pH 7.4 with NaOH), 0.1 mM $FeSO_4$, 0.276 mM Na_2SO_4, 0.5 μM $CaCl_2$, 0.523 mM $MgCl_2$ and also micronutrient mixtures as used in Cayley et al[50]. The carbon sources and nitrogen sources were varied to create different nutrient limitation. Detailed nutrient conditions are the same as Dai et al[20].

Cell growth

Cell growth was always performed in a 37°C air bath shaker (200 rpm). The cell growth procedure contained three steps: seed culture, pre-culture and experimental culture. Cells from a fresh colony in the LB plate were inoculated into LB medium and grown for several hours as seed culture. Seed cultures were then transferred into the medium of the final experimental culture (e.g. glucose minimal medium or glycerol minimal medium with certain antibiotic concentration) as precultures. Inoculation of the pre-culture with washed seed culture was selected such that the pre-culture grown overnight were still growing before reaching saturation on the morning of the experiment. Cells in the pre-culture were kept growing exponentially for at least ten doublings (at least five for growth rates below 0.4 h^{-1}). Exponentially growing pre-culture were inoculated into the final experimental medium at an initial OD_{600} ~ 0.015 as experimental culture. For each condition, we took 6–8 OD_{600} points (at the range of 0.05 to 0.5) to get an exponential growth curve for the calculation of growth rate. The values of OD_{600} were measured by a Thermo Sci genesys30 spectrophotometer.

For the growth measurement of FL56 cells, the seed culture and pre-culture were grown without cTc; the final experimental cultures of FL56 cells (either with or without fusidic acid) were first growing exponentially to OD_{600}~0.3, then cTc was added to induced $RelA^+$ expression, OD_{600} data points were taken at a 5-min interval to record growth arrest. IPTG was added at 20 min after the onset of growth arrest.

Measurement of translation elongation speed

Measurements of the translational elongation speed of *E. coli* were based on the classical *lacZ* induction assay with a 10-s initiation time calibrated, as described in Dai et al[19,20].

Transcription kinetics measurement

E. coli cells were exponentially growing to OD_{600} ~0.4 followed by the induction of *lac* operon expression through addition of 5 mM isopropyl-β-D-thiogalactoside (IPTG). Immediately after the IPTG induction, 2 mL of cell culture was withdrawn at a 10- or 15-s interval and transferred into a 5-mL plastic tube containing 2 mL stop solution containing 60% ethanol, 2% phenol and 10 mM EDTA (pre-cooled in −20 °C). The total cellular RNA was then extracted with a bacterial total RNA extraction kit (TianGen, China). The final concentration of RNA was then measured with a NanoDrop-1000 micro-spectrophotometer. 1-μg total cellular RNA was used for cDNA synthesis with a first-strand cDNA synthesis reverse transcriptase kit (Tsingke biotech, China). The qRT-PCR reaction was performed based on the Super-premix SYBR green Plus kit (Yeasen Biotech, Shanghai, China) using Bio-rad CFX96 Touch real-time PCR system. Detailed qRT-PCR reaction protocol is as follows: 95°C for 15 min, followed by 40 cycles of 95°C for 10 s, 60°C for 20 s, and 72°C for 30 s. The *lacZ* mRNA abundance of a sample taken immediately before IPTG addition (referred to as “basal sample”), M(0), was set as “1”. The relative *lacZ* mRNA abundance in each time point, M(t), equals to $2^{Cq0-Cqt}$, where Cq0 means the Cq value of basal sample and Cqt means the Cq value at each time point. The *lacZ* mRNA abundance was plotted with the time to obtain the transcriptional kinetics curve from which the transcriptional time of seven mRNA sub-regions (detected by the corresponding seven pairs of primers) can be

deduced. The linear range of each induction kinetic was fit with linear line. The best fit of the each linear line was described as: $y = a \cdot x - b$ where a (the slope of the line) denoted the relative mRNA transcription rate of each mRNA sub-regions; the transcriptional time of each position, T_j, equals to $(1 + b)/a$. The position (the position of the 3' nucleotide within he transcriptional start site) of the seven mRNA was plotted with the transcriptional time to deduce the transcriptional elongation speed (as exemplified in Figure 1A and 1B). For each condition, the average and standard error of three multiple-probes data from three independent cultures in parallel was calculated as the final data listed in supplementary table (Table S1 and Table S2). Instead, the error shown in related figures of the main text corresponds to the uncertainty of linear fit of single-round multiple probe data. For the experiments with bicyclomycin (Bcm), cell were first exponentially growing to OD_{600}~0.3, 20 μg/mL Bcm was added to exponentially growing cells; after 15s, IPTG was added to induce the transcription of *lacZ* mRNA.

Total RNA measurement

The total RNA content measurement was the same as described in Dai et al[20]. Three total RNA samples were separately taken from the same three independent cultures (above) for transcriptional kinetics measurement before addition of IPTG. Data of total RNA value are averages of triplicates.

Total protein measurement

The total protein content measurement was the same as described in Dai et al[20]. Three total protein samples were separately taken from the same three independent cultures (above) for transcriptional kinetics measurement before addition of IPTG. Data of total protein are averages of triplicates.

Measurement of ppGpp pools in FL56 strain by UPLC-MS

The measurement of cellular ppGpp level is based on the UPLC-MS method as described in Yuta et al[51]. In brief, the culture of FL56 strain was growing exponentially to OD600≈0.4. 2 mL cell sample was taken and immediately collected by centrifugation for 0.5 min at 14000 rpm at 4 °C and washed once by ice-cold water. Cells were then crushed in 3 mL pre-cooled 2 M formic acid at 30 min and subjected to solid-phase extraction (SPE) protocol as detailed in Ref.[51]. The UPLC-MS experiment was performed with Thermo Scientific TSQ Fortis triple quadrupole mass spectrometer.

Supplementary Material

Refer to Web version on PubMed Central for supplementary material.

Acknowledgement

We are grateful to Minsu Kim and Rohan Balakrishnan for discussion. XD and MZ acknowledge the support of the National Natural Science Fund of China (No. 31700089, No. 31700039 and No. 31870028) and by CCNU (self-determined research funds of CCNU from the colleges' basic research and operation of MOE, CCNU18QN028, CCNU18KFY01, CCNU19TS028 and CCNU18ZDPY05). MM and TH acknowledge the support of the NIH through Grant R01GM095903.

REFERENCES

1. Gowrishankar J & Harinarayanan R Why is transcription coupled to translation in bacteria? Mol Microbiol 54, 598–603, doi:10.1111/j.1365-2958.2004.04289.x (2004). [PubMed: 15491353]
2. McGary K & Nudler E RNA polymerase and the ribosome: the close relationship. Curr Opin Microbiol 16, 112–117, doi:10.1016/j.mib.2013.01.010 (2013). [PubMed: 23433801]
3. Vogel U & Jensen KF The RNA chain elongation rate in Escherichia coli depends on the growth rate. J Bacteriol 176, 2807–2813 (1994). [PubMed: 7514589]
4. Proshkin S, Rahmouni AR, Mironov A & Nudler E Cooperation between translating ribosomes and RNA polymerase in transcription elongation. Science 328, 504–508, doi:10.1126/science.1184939 (2010). [PubMed: 20413502]
5. Newton WA, Beckwith JR, Zipser D & Brenner S Nonsense mutants and polarity in the lac operon of Escherichia coli. J Mol Biol 14, 290–296 (1965). [PubMed: 5327654]
6. Elgamal S, Artsimovitch I & Ibba M Maintenance of Transcription-Translation Coupling by Elongation Factor P. MBio 7, doi:10.1128/mBio.01373-16 (2016).
7. Adhya S & Gottesman M Control of transcription termination. Annu Rev Biochem 47, 967–996, doi:10.1146/annurev.bi.47.070178.004535 (1978). [PubMed: 354508]
8. Richardson JP Preventing the synthesis of unused transcripts by Rho factor. Cell 64, 1047–1049 (1991). [PubMed: 2004415]
9. Kohler R, Mooney RA, Mills DJ, Landick R & Cramer P Architecture of a transcribing-translating expressome. Science 356, 194–197, doi:10.1126/science.aal3059 (2017). [PubMed: 28408604]
10. Miller OL Jr., Hamkalo BA & Thomas CA Jr. Visualization of bacterial genes in action. Science 169, 392–395 (1970). [PubMed: 4915822]
11. Demo G et al. Structure of RNA polymerase bound to ribosomal 30S subunit. Elife 6, doi:10.7554/eLife.28560 (2017).
12. Fan H et al. Transcription-translation coupling: direct interactions of RNA polymerase with ribosomes and ribosomal subunits. Nucleic Acids Res 45, 11043–11055, doi:10.1093/nar/gkx719 (2017). [PubMed: 28977553]
13. Burmann BM et al. A NusE:NusG complex links transcription and translation. Science 328, 501–504, doi:10.1126/science.1184953 (2010). [PubMed: 20413501]
14. Saxena S et al. Escherichia coli transcription factor NusG binds to 70S ribosomes. Molecular Microbiology, doi:doi:10.1111/mmi.13953 (2018).
15. Burmann BM et al. An alpha helix to beta barrel domain switch transform s the transcription factor RfaH into a translation factor. Cell 150, 291–303, doi:10.1016/j.cell.2012.05.042 (2012). [PubMed: 22817892]
16. Chen M & Fredrick K Measures of single-versus multiple-round translation argue against a mechanism to ensure coupling of transcription and translation. Proc Natl Acad Sci U S A 115, 10774–10779, doi:10.1073/pnas.1812940115 (2018). [PubMed: 30275301]
17. Bremer H & Dennis PP Modulation of chemical composition and other parameters of the cell at different exponential growth rates Escherichia coli and Salmonella, ed Neidhardt FC (Am Soc Microbiol, Washington,DC), 2nd Ed, 1553–1569 (1996).
18. Iyer S, Park BR & Kim M Absolute quantitative measurement of transcriptional kinetic parameters in vivo. Nucleic Acids Res 44, e142, doi:10.1093/nar/gkw596 (2016). [PubMed: 27378780]
19. Dai X et al. Slowdown of Translational Elongation in Escherichia coli under Hyperosmotic Stress. MBio 9, doi:10.1128/mBio.02375-17 (2018).
20. Dai X et al. Reduction of translating ribosomes enables Escherichia coli to maintain elongation rates during slow growth. Nat Microbiol 2, 16231 (2016). [PubMed: 27941827]
21. Zhu M, Dai X & Wang YP Real time determination of bacterial in vivo ribosome translation elongation speed based on LacZα complementation system. Nucleic Acids Research 44, e155–e155 (2016). [PubMed: 27903884]
22. Schleif R, Hess W, Finkelstein S & Ellis D Induction kinetics of the L-arabinose operon of Escherichia coli. J Bacteriol 115, 9–14 (1973). [PubMed: 4577756]

23. Bennett PM & Maaloe O The effects of fusidic acid on growth, ribosome synthesis and RNA metabolism in Escherichia coli. J Mol Biol 90, 541–561 (1974). [PubMed: 4217388]
24. Seo HS et al. EF-G-dependent GTPase on the ribosome. conformational change and fusidic acid inhibition. Biochemistry 45, 2504–2514, doi:10.1021/bi0516677 (2006). [PubMed: 16489743]
25. Richardson LV & Richardson JP Rho-dependent termination of transcription is governed primarily by the upstream Rho utilization (rut) sequences of a terminator. J Biol Chem 271, 21597–21603 (1996). [PubMed: 8702947]
26. Graham JE & Richardson JP rut Sites in the nascent transcript mediate Rho-dependent transcription termination in vivo. J Biol Chem 273, 20764–20769 (1998). [PubMed: 9694820]
27. Ruteshouser EC & Richardson JP Identification and characterization of transcription term ination sites in the Escherichia coli lacZ gene ☆. J Mol Biol 208, 23–43 (1989). [PubMed: 2475637]
28. Harvey RJ & Koch AL How partially inhibitory concentrations of chloramphenicol affect the growth of Escherichia coli. Antimicrob Agents Chemother 18, 323–337 (1980). [PubMed: 6160809]
29. Maguire BA Inhibition of bacterial ribosome assembly: a suitable drug target? Microbiol Mol Biol Rev 73, 22–35, doi:10.1128/MMBR.00030-08 (2009). [PubMed: 19258531]
30. Hui S et al. Quantitative proteomic analysis reveals a simple strategy of global resource allocation in bacteria. Mol Syst Biol 11, 784, doi:10.15252/msb.20145697 (2015). [PubMed: 25678603]
31. Potrykus K & Cashel M (p)ppGpp: still magical? Annu Rev Microbiol 62, 35–51, doi:10.1146/annurev.micro.62.081307.162903 (2008). [PubMed: 18454629]
32. Vogel U, Sorensen M, Pedersen S, Jensen KF & Kilstrup M Decreasing transcription elongation rate in Escherichia coli exposed to amino acid starvation. Mol Microbiol 6, 2191–2200 (1992). [PubMed: 1406259]
33. Vogel U & Jensen KF Effects of guanosine 3',5'-bisdiphosphate (ppGpp) on rate of transcription elongation in isoleucine-starved Escherichia coli. J Biol Chem 269, 16236–16241 (1994). [PubMed: 8206927]
34. Iyer S, Le D, Park BR & Kim M Distinct mechanisms coordinate transcription and translation under carbon and nitrogen starvation in Escherichia coli. Nature Microbiology 3, 741 (2018).
35. Kingston RE, Nierman WC & Chamberlin MJ A direct effect of guanosine tetraphosphate on pausing of Escherichia coli RNA polymerase during RNA chain elongation. J Biol Chem 256, 2787–2797 (1981). [PubMed: 7009598]
36. Furman R, Sevostyanova A & Artsimovitch I Transcription initiation factor DksA has diverse effects on RNA chain elongation. Nucleic Acids Res 40, 3392–3402, doi:10.1093/nar/gkr1273 (2012). [PubMed: 22210857]
37. Klumpp S, Zhang Z & Hwa T Growth rate-dependent global effects on gene expression in bacteria. Cell 139, 1366–1375, doi:10.1016/j.cell.2009.12.001 (2009). [PubMed: 20064380]
38. Schreiber G et al. Overexpression of the relA gene in Escherichia coli. J Biol Chem 266, 3760–3767 (1991). [PubMed: 1899866]
39. Svitil AL, Cashel M & Zyskind JW Guanosine tetraphosphate inhibits protein synthesis in vivo. A possible protective mechanism for starvation stress in Escherichia coli. J Biol Chem 268, 2307–2311 (1993). [PubMed: 8428905]
40. Hernandez VJ & Bremer H Guanosine tetraphosphate (ppGpp) dependence of the growth rate control of rrnB P1 promoter activity in Escherichia coli. J Biol Chem 265, 11605–11614 (1990). [PubMed: 2114400]
41. Ryals J, Little R & Bremer H Control of rRNA and tRNA syntheses in Escherichia coli by guanosine tetraphosphate. J Bacteriol 151, 1261–1268 (1982). [PubMed: 6179924]
42. Shibuya M & Kaziro Y Studies on stringent control in a cell-free system. Regulation by guanosine-5'-diphosphate-3'-diphosphate of the synthesis of elongation factor Tu. J Biochem 86, 403–411 (1979). [PubMed: 158010]
43. Hernandez VJ & Bremer H Guanosine tetraphosphate (ppGpp) dependence of the growth rate control of rrnB P1 promoter activity in Escherichia coli. Journal of Biological Chemistry 265, 11605–11614 (1990). [PubMed: 2114400]

44. Zhu M & Dai X Growth suppression by altered (p)ppGpp levels results from non-optimal resource allocation in Escherichia coli. Nucleic Acids Res 47, 4684–4693, doi:10.1093/nar/gkz211 (2019). [PubMed: 30916318]
45. Scott M, Klumpp S, Mateescu EM & Hwa T Emergence of robust growth laws from optimal regulation of ribosome synthesis. Mol Syst Biol 10, 747, doi:10.15252/msb.20145379 (2014). [PubMed: 25149558]
46. Siibak T et al. Erythromycin- and chloramphenicol-induced ribosomal assembly defects are secondary effects of protein synthesis inhibition. Antimicrob Agents Chemother 53, 563–571, doi: 10.1128/AAC.00870-08 (2009). [PubMed: 19029332]
47. Scott M, Gunderson CW, Mateescu EM, Zhang Z & Hwa T Interdependence of cell growth and gene expression: origins and consequences. Science 330, 1099–1102, doi:10.1126/science. 1192588 (2010). [PubMed: 21097934]
48. Saxena S & Gowrishankar J Modulation of Rho-dependent transcription termination in Escherichia coli by the H-NS family of proteins. J Bacteriol 193, 3832–3841, doi:10.1128/JB.00220-11 (2011). [PubMed: 21602341]
49. Nieto JM, Bailey MJ, Hughes C & Koronakis V Suppression of transcription polarity in the Escherichia coli haemolysin operon by a short upstream element shared by polysaccharide and DNA transfer determinants. Mol Microbiol 19, 705–713 (1996). [PubMed: 8820641]
50. Cayley S, Lewis BA, Guttman HJ & Record MT Jr. Characterization of the cytoplasm of Escherichia coli K-12 as a function of external osmolarity. Implications for protein-DNA interactions in vivo. J Mol Biol 222, 281–300 (1991). [PubMed: 1960728]
51. Ihara Y, Ohta H & Masuda S A highly sensitive quantification method for the accumulation of alarmone ppGpp in Arabidopsis thaliana using UPLC-ESI-qMS/MS. Journal of Plant Research 128, 511–518 (2015). [PubMed: 25752614]

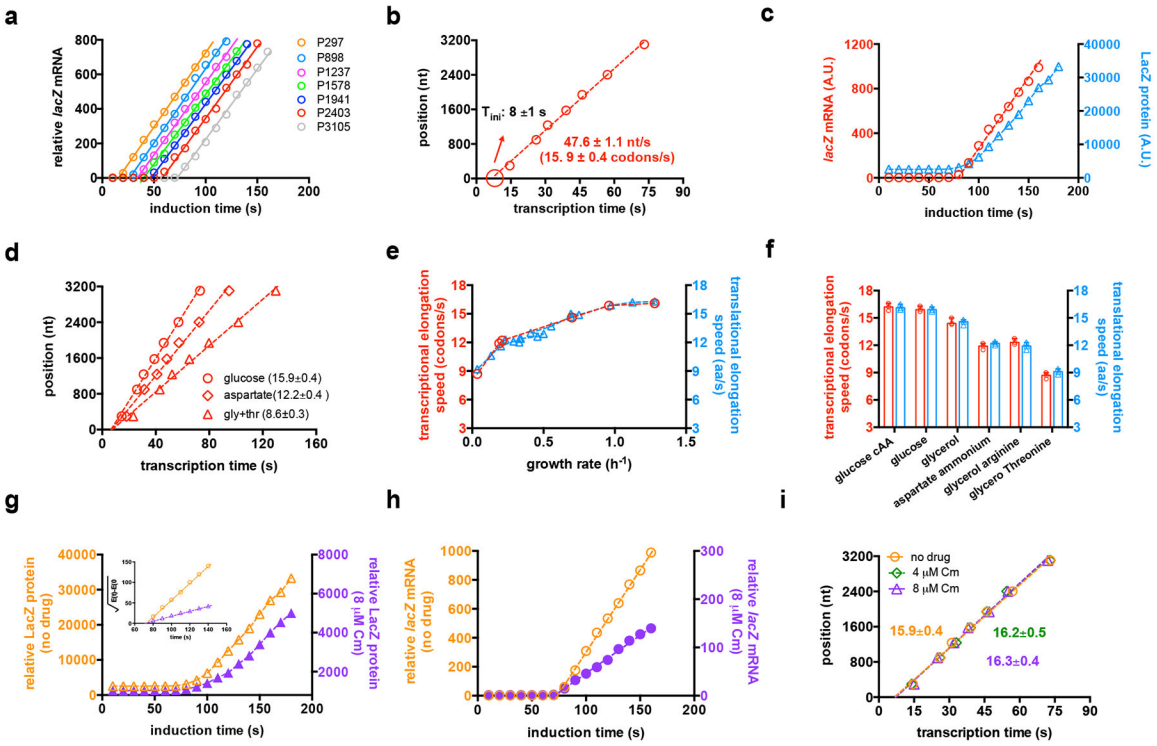

Figure 1: qRT-PCR based characterization of transcriptional elongation speed.

(a) *lacZ* mRNA induction curves of *E. coli* K-12 NCM3722 cells grown exponentially in MOPS glucose minimal medium. Seven pairs of primers were used to detect the abundances of different *lacZ* mRNA sub-regions. The rising component of each mRNA induction curve was fitted to a line. **(b)** Transcriptional elongation speed obtained by plot the waiting time against the probe position of each primer pair. The data are fitted to a linear line, whose slope gives the transcriptional elongation speed and the X-intercept gives the time needed to initiate the *lacZ* mRNA transcription after addition of IPTG. The errors denote the uncertainty of the linear fit. **(c)** The induction curve of intact *lacZ* mRNA (detected by P3105 primer) is plotted together with the LacZ induction curve. **(d)** The multi-probe transcriptional elongation analysis done at 3 other growth conditions as indicated by the legend. The errors denote the uncertainty of the linear fit. **(e)** Growth-rate dependent transcriptional and translational elongation speeds under nutrient limitation. Transcriptional elongation speeds are listed in supplementary table 1. Data of translational elongation speed is from Ref.[20]. **(f)** Summary of transcriptional and translational elongation speeds in different growth conditions. Data were shown as media with standard deviation of three biological replicates. **(g)** LacZ induction curve of cells growing in glucose minimal medium with/without 8 μM Cm. The inset shows the corresponding Schleif plots. **(h)** The induction curve of the intact *lacZ* mRNA (detected by P3105 primer) of cells growing in glucose minimal medium with/without 8 μM Cm. **(i)** Multiple-probe transcriptional elongation analysis of cells growing in glucose medium with 4 or 8 μM Cm. Data of no-drug condition is the same as in panel b. The errors in panel i denote the uncertainty of the linear fit. Data shown in panel a, c, e, g and h have been repeated three times independently with similar

results. Data shown in panel b, d and i show the analytic result of a typical multiple-probe curve such as panel a and we repeated three times independently with similar results.

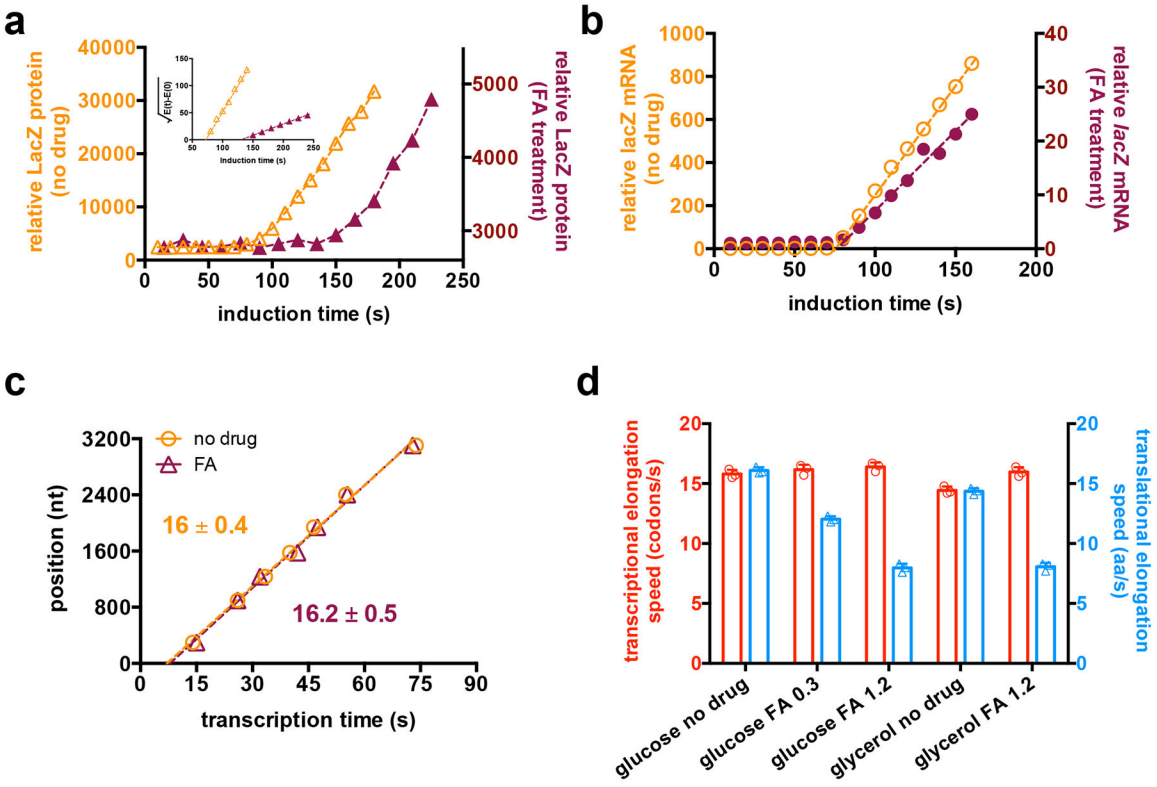

Figure 2. Transcriptional elongation in conditions of reduced translational elongation by fusidic acid.

(a) The induction curve of LacZ protein for *E. coli* AS19 strain growing in glucose minimal medium with/without 1.2 μg/mL FA. Inset shows the Schleif plots. **(b)** The induction curve of full-length *lacZ* mRNA for *E. coli* AS19 growing in glucose minimal medium with/without 1.2 μg/mL FA. **(c)** Multiple-probe analysis of transcriptional elongation for *E. coli* AS19 cells growing in glucose medium with 1.2 μg/mL FA. **(d)** Summary of transcriptional and translational elongation speeds for cells subjected to fusidic acid treatment. Data shown in panel a and b have been repeated three times independently with similar results. Data shown in panel b, d and i show the analytic result of a typical multiple-probe curve and we repeated three times independently with similar results. Data of panel d were shown as media with standard deviation of three biological replicates.

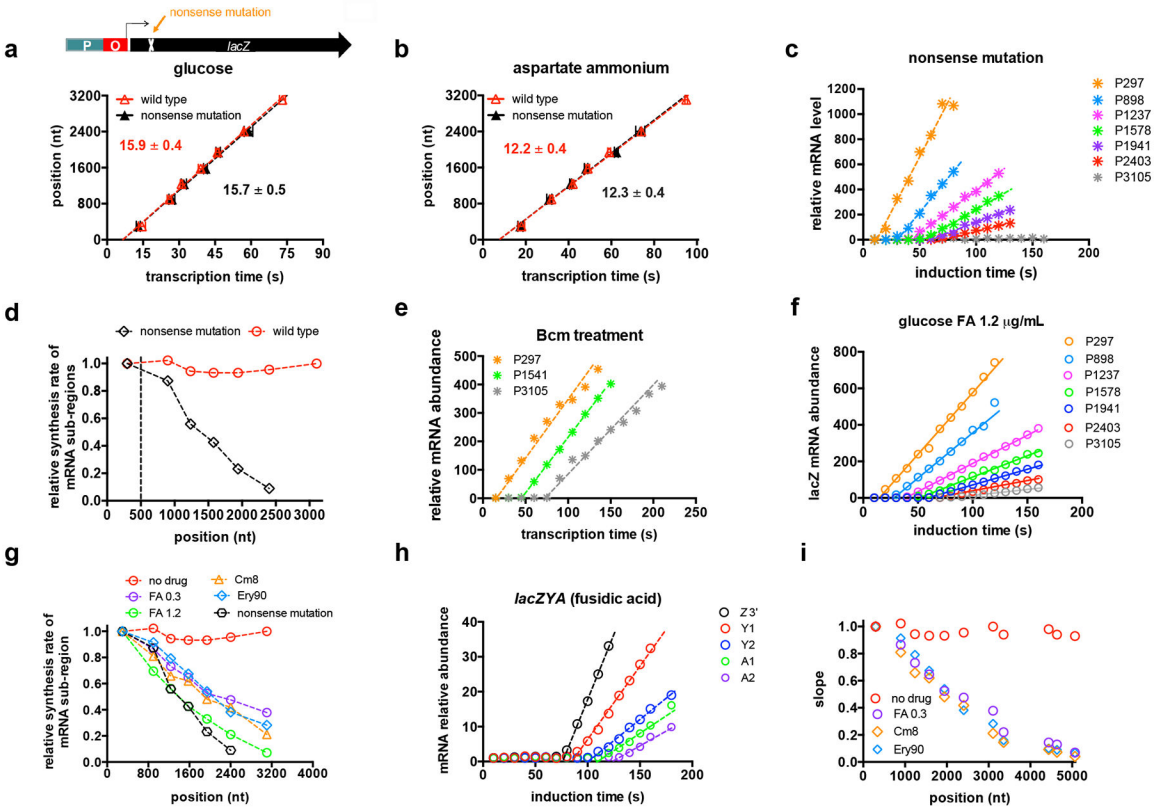

Figure 3. The *lacZ* mRNA transcription induction kinetics upon nonsense mutation and antibiotic treatment.

(a) Transcriptional elongation analysis of nonsense-mutated *lacZ* mRNA of FL57 strain growing in glucose medium. **(b)** Same as panel a, but growing slowly in medium with aspartate as the sole carbon source. In all cases, the error shown denotes the uncertainty of the linear fit. Data shown in panel a and b show the analytic result of a typical multiple-probe curve and we repeated three times independently with similar results. **(c)** The mRNA induction curves of *lacZ* with a nonsense mutation in glucose medium. **(d)** The relative synthesis rate of each mRNA sub-regions (the slope of the linear induction curve) versus the hybridization location of the primers in the *lacZ* mRNA molecules. The position of the transcriptional start site *of lacZ* mRNA is set as location "zero". The synthesis rate of the 5' mRNA sub-region detected by P297 primer is set as "1". Data of native *lacZ* gene and nonsense mutated *lacZ* corresponds to Figure 1a and panel c, respectively. **(e)** Transcription kinetics of nonsense-mutated *lacZ* mRNA of *E. coli* cells treated with 20 μg/mL bicyclomycin (Bcm). Bcm was added to exponentially growing cells; after 15 s, IPTG was added to induce the transcription of *lacZ* mRNA. **(f)** The mRNA induction curves of *lacZ* in *E. coli* cells growing with 1.2 μg/mL fusidic acid. **(g)** The relative synthesis rate of each mRNA sub-regions versus the hybridization location of the primers in the *lacZ* mRNA molecules in drug conditions. **(h)** Transcriptional premature termination of the entire *lac* operon under FA treatment. Cells were grown in glucose minimal medium with 0.3 μg/mL fusidic acid. Z 3' corresponds to the synthesis kinetics of the 3' end (tail) of *lacZ* mRNA using P3105 primer. Four additional primers were used for detect the synthesis rate of the near 5' head sub-region and near-3' sub-region of both *lacY* (Y1 and Y2) and *lacA* mRNA

(A1 and A2). **(i)** The relative synthesis rate of each mRNA sub-regions (the slope of the linear induction curve) versus the hybridization location of the primers in the entire *lac* operon in drug conditions. Data shown in panel c to i have been repeated three times independently with similar results.

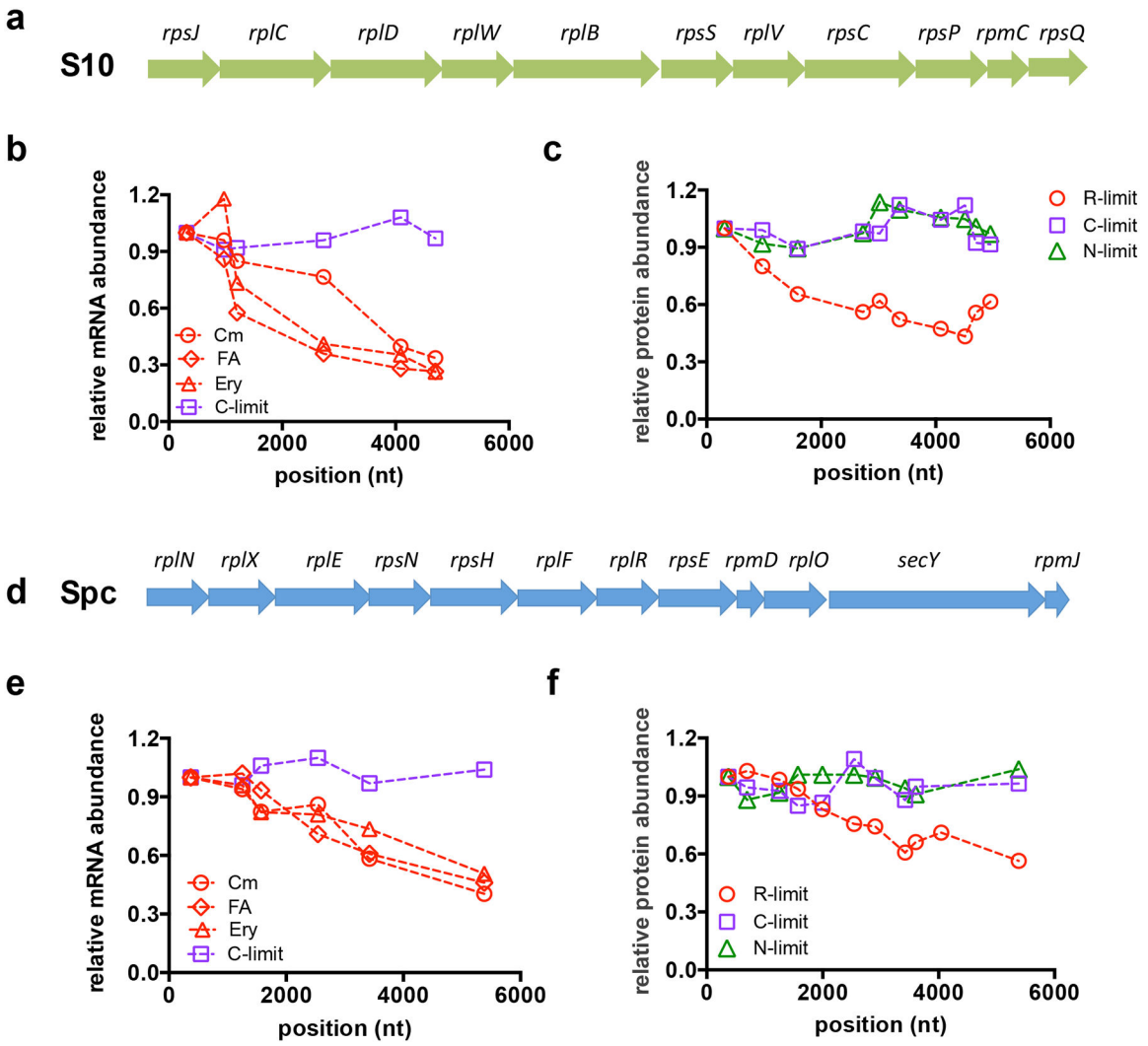

Figure 4. Expression polarity of the ribosomal protein (r-protein) operon under antibiotic treatment.

(a) The ribosomal S10 operon. **(b)** The relative mRNA abundance of S10 r-protein upon 1.2 μg/mL FA, 90 μg/mL Ery, 8 μM Cm and carbon limitation. FA denotes fusidic acid; Ery denotes erythromycin. **(c)** The correlation between the S10 operon r-protein abundance with the location of each r-protein under 8 μM Cm, carbon limitation and nitrogen limitation. The transcriptional start site of S10 operon is set as "zero". The location of each r-protein corresponds to the distance (nt) between its stop codon and zero site. Data of RpsJ abundance in each set is set as "1". **(d)** Spc operon. **(e)** The relative mRNA abundance of Spc r-protein upon antibiotic treatment and carbon limitation. FA denotes fusidic acid; Ery denotes erythromycin. **(f)** The correlation between Spc operon r-protein abundance with the location of each r-protein under 8 μM Cm or carbon limitation. The transcriptional start site of Spc operon is set as "zero". The location of each r-protein corresponds to the distance (nt) between its stop codon and zero sites. Data of RplN abundance in each set is set as "1". Proteomic data in panel c and f originate from Ref.[30] with three biological replicates. Data shown in panel b and e have been repeated three times independently with similar results.

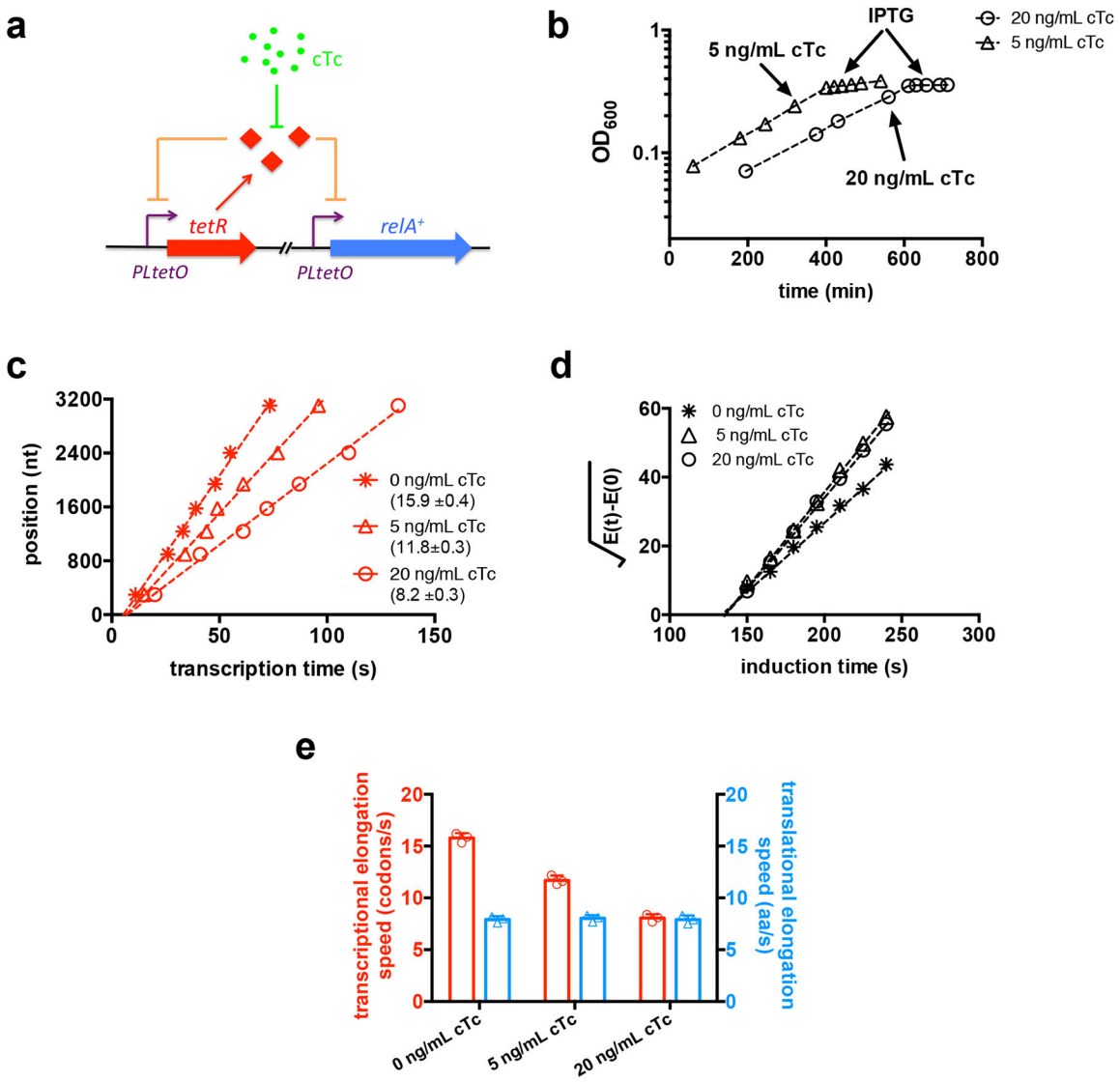

Figure 5. Effect of ppGpp on transcriptional elongation.

(a) The ppGpp upregulation strain, FL56, derived from AS19, harbors titratable expression of the *relA*$^+$ gene (encoding constitutively active RelA protein, encoding the N-terminal 455 residues of the native RelA protein) under the control of the P_{LtetO} promoter located on a pZE11 plasmid. The expression of RelA$^+$ protein is controlled by the TetR repressor (also driven by the P_{LtetO} promoter located on a pZA31 plasmid), which can be de-repressed by chlortetracycline (cTc). See Methods. **(b)** Expression of RelA$^+$ protein through the addition of 5 or 20 ng/mL cTc in glucose medium with 1.2 μg/mL fusidic acid (FA) results in rapid growth arrest within less than half an hour. IPTG was added to the cultures at ~20 minutes after the onset of growth arrest to induce the *lacZ* expression for the characterization of transcriptional and translational elongation speeds in panel c. **(d)** Multi-probe transcriptional elongation analysis for FL56 strain grown in glucose medium with 1.2 mg/mL FA, 20 min after different levels of RelA$^+$ induction (by cTc addition). The error denotes the uncertainty of the linear fit. **(d)** Schleif plot of LacZ protein induction curve for FL56 strain treated in

the same way as panel c. **(e)** Summary of the effect of $RelA^+$ induction on the transcriptional-translational elongation speeds for FL56 cells characterized in panels b and c. Data shown in panel b and d have been repeated three times independently with similar results. Data shown in panel c show the analytic result of a typical multiple-probe curve and we repeated three times independently with similar results. Data of panel e were shown as media with standard deviation of three biological replicates.

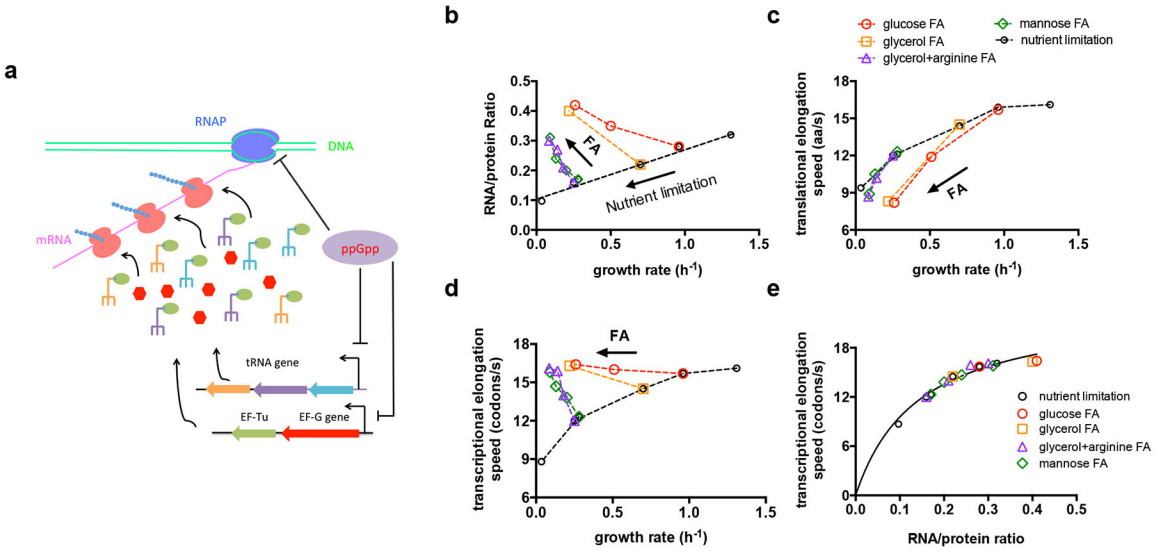

Figure 6. Coordination of transcriptional and translational elongation under nutrient limitation.

(a) Model of ppGpp-mediated coordination of transcriptional and translational elongation. Under nutrient limitation, the cellular ppGpp pool increases, inhibiting the synthesis of translation substrates such as tRNA, EF-Tu and EF-G, causing slowdown of translational elongation. Concomitantly, ppGpp exerts inhibitory effect on transcriptional elongation of mRNA by RNAP; see supplementary Figure 17 for detailed explanation. **(b)** The RNA/protein ratio of AS19 strain is plotted against growth rate under both nutrient limitations and fusidic acid treatment. Each color represents a fixed nutrient source supplemented with different doses of fusidic acid. The nutrient limitation case (black circles) represents different nutrient conditions without FA. The slowest growth rate was obtained using glycerol with threonine as the sole nitrogen source; it supports a doubling time of ~20 h. **(c)** Translational elongation speed plotted against growth rate under the same growth condition as described in panel b. **(d)** Transcriptional elongation speed plotted against growth rate; same growth conditions as panel b. **(e)** Transcriptional elongation speed plotted against RNA/Protein (*R/P*) ratio for the same growth conditions. The transcriptional elongation speed of all the data points in panel d is used as the y-axis; the *R/P* data in panel b are used as the x-axis. Black line is a least-square fit to the Michaelis-Menten relation. Data points shown in panel b to e have been repeated three times independently with similar results.